ChemElectroChem

Research Article
doi.org/10.1002/celc.202201037

Chemistry Europe
European Chemical Societies Publishing

www.chemelectrochem.org

Role of Superoxide and Singlet Oxygen on the Oxygen Reduction Pathways in Li–O_2 Cathodes at Different Li^+ Ion Concentration**

Alvaro Y. Tesio, Walter Torres, Matías Villalba, Federico Davia, María del Pozo, Daniel Córdoba, Federico J. Williams, and Ernesto J. Calvo*[a]

Dedicated to Prof. Plamen Atanasov

The oxygen reduction reaction (ORR) on Au electrodes has been studied in DMSO at different Li^+ concentrations. In-operando fluorescence decay of 9,10-dimethyl anthracene (DMA) has shown that disproportionation of lithium superoxide $Li^+O_2^-$ into Li_2O_2 and O_2 leads to an increasing fraction of very reactive singlet oxygen ($^1O_2$) at high lithium concentration. Singlet oxygen has been identified as the major cause of parasitic reactions leading to capacity fading and high charge overpotential of Li–O_2 batteries. Rotating ring-disk electrode shows quantitative formation of soluble superoxide at low Li^+ concentration, a decrease in superoxide yield at high Li^+ concentrations is consistent with electrochemical quartz crystal microbalance (EQCM) evidence of Li_2O_2 deposits. Differential electro chemical mass spectrometry (DEMS) confirms oxygen depletion at the electrode surface during ORR, and O_2 evolution during oxidation at 3.1 V (vs. Li/Li^+ in DMSO). The spurious solvent decomposition due to the very reactive $^1O_2$ from superoxide disproportionation is revealed by gravimetric EQCM of insoluble by-products. Furthermore, DEMS provides evidence of CO_2 gas evolution from decomposition of Li_2CO_3 by-product at 3.7 V (vs. Li/Li^+ in DMSO). Preliminary in-operando full discharge-charge tests of a Li–O_2 battery with $^1O_2$ quencher azide resulted in stable cycling, enhanced capacity and full charge recovery in a round trip.

Introduction

The rechargeable lithium air battery introduced by Abraham in 1996[1] was discovered by serendipity[2] and exhibits an energy density comparable to fossil fuels.[3] However, it suffers from capacity fading and the high charging overpotential due to parasitic reactions of the O_2 reduction products with solvents and electrolyte.[4,5] In practice the reversibility of the Li–O_2 battery as measured by the ratio of evolved and consumed O_2 does not reach more than 80% due to parasitic reactions.[6]

A recent comprehensive review on the Lithium-Oxygen Batteries[7] describes the status of a large body of results. Oxygen reduction to Li_2O_2 on discharge involves soluble superoxide (O_2^-), which has been shown to react with electrolyte and carbon electrodes upon disproportionation of $[Li^+O_2^-]_{DMSO}$ at the onset potential of the ORR and adsorbed LiO_2 at higher overpotentials.[8] In the presence of Li^+ ions the reaction yields $^1O_2$ which is the cause of spurious reactions that lead to solvent and electrolyte degradation.[6] The role of superoxide in Li–O_2 battery cathodes has been a recent matter of controversy[9] and discussion.[10]

Dimethyl sulfoxide (DMSO) is a high donor number (DN) solvent which stabilizes the lithium superoxide ion pair.[11] DMSO has been reported as solvent in Li-air battery to improve performance and stability.[10,12] However, the stability of DMSO[4,10,11] in Li–O_2 batteries has been questioned since side products such as LiOH,[13,14] dimethyl sulfone,Li_2SO_3 and Li_2SO_4[15–17] have been detected at the cathode.

With respect to electrolyte stability, superoxide radical anion (O_2^-) plays a role as an important intermediate: Superoxide is stable in electrolytes containing large cations, such as tetra butyl ammonium (TBA^+) with formation of solvated non-contact ionic pairs, $[TBA^+O_2^-]_{DMSO}$.[18] But in the presence of small lithium cations molecular dynamics simulations have shown that they are highly solvated $Li(DMSO)_4^+$[19] and form soluble $[Li^+O_2^-]_{DMSO}$ ion pairs during the ORR that have been detected in solution by RRDE[20–24] and on Au surfaces by Raman spectroscopy.[23,25]

Under these conditions it has been established that at low overpotentials lithium superoxide undergoes disproportionation into Li_2O_2 and molecular O_2.[23,26] At higher overpotentials further electron and Li^+ ion transfer yield the insoluble Li_2O_2 end product which has been confirmed by Raman spectroscopy[23,27] and gravimetric EQCM.[17,26] A fraction of the O_2 that evolves from lithium superoxide disproportionation is the highly reactive singlet oxygen as has recently been shown with electron spin resonance[28] and electrochemical

[a] Dr. A. Y. Tesio, Dr. W. Torres, Dr. M. Villalba, Dr. F. Davia, Dr. M. del Pozo, D. Córdoba, Prof. F. J. Williams, Prof. E. J. Calvo
INQUIMAE (CONICET), DQIAyQF, Facultad de Ciencias Exactas y Naturales
Universidad de Buenos Aires
Buenos Aires, 1428, Argentina
E-mail: calvo@qi.fcen.uba.ar
Homepage: http://www.inquimae.fcen.uba.ar/

[**] *An invited contribution to the Plamen Atanassov Festschrift*

Supporting information for this article is available on the WWW under https://doi.org/10.1002/celc.202201037

fluorescence experiments.[29–31] Based on the Raman shifts of superoxide features Johnson et al.[23] have suggested in addition to the soluble $[Li^+O_2^-]_{DMSO}$ (1105–1110 cm^{-1}) the formation of LiO_2 (1125–1130 cm^{-1}) adsorbed on Au electrodes during ORR in DMSO. The adsorbed species LiO_2 has shorter O–O bond length than soluble $[Li^+O_2^-]_{DMSO}$ and thus more covalent character; it is very reactive and can be further reduced to peroxide at higher overpotentials. The group of Peng et. al.[32] succeeded to prepare LiO_2 in liquid NH_3 at cryogenic temperatures (−196 °C) and characterized it spectroscopically. Furthermore, a mechanistic study of the ORR on an Au electrode in Li^+ containing dimethyl sulfoxide (DMSO) has described the formation of $[Li^+O_2^-]_{DMSO}$ at the onset potential of the ORR and adsorbed LiO_2 at higher overpotentials.[8]

In the presence of lithium ions, superoxide radical anion undergoes disproportionation into Li_2O_2 insoluble in DMSO and soluble O_2, a fraction of which has been found to be the extremely reactive singlet oxygen ($^1O_2$ or $^1\Delta_g$) as well as triplet oxygen ($^3O_2$) (Reaction 1).[30,31]

$$\left[Li^+O_2^-\right]_{DMSO} + \left[Li^+O_2^-\right]_{DMSO} \rightarrow Li_2O_2 \downarrow + x^1O_2 + (1-x)^3O_2 \quad (1)$$

where $[Li^+O_2^-]_{DMSO}$ is a surface solvated superoxide ion pair.

Photochemically generated single oxygen forms lithium carbonate upon exposure to 0.1 M $LiClO_4$ in DME electrolyte by spurious reaction with the solvent[29] and singlet oxygen generated by photoexcitation of Rose Bengal also reacts with carbonate solvents in Li-ion batteries.[33] Furthermore,$^1O_2$ has been also recognized to contribute to deactivation of redox mediators.[34]

A shift in the standard potential of the couple O_2/O_2^- ($E^0_{O2/LiO2} = 2.65$ V) to that of O_2/Li_2O_2 pair ($E^0_{O2/Li2O2} = 2.96$ V) on replacing TBA^+ with Li^+ in DMSO has been reported from cyclic voltammetry experiments in DMSO electrolyte.[23] Addition of Li^+ ions to a stable solution of electrochemically generated O_2^- in $TBA^+PF_6^-$ in DMSO has shown a shift of the open circuit potential to positive values from the O_2/O_2^- towards the O_2/Li_2O_2 potential with simultaneous detection of Li_2O_2 by EQCM and AFM due to superoxide disproportionation.[26] Similar experiments with fluorescence quenching demonstrated the evolution of singlet oxygen during the disproportionation of lithium superoxide.[30] Furthermore, O_2 bond cleavage and oxygen atom scrambling during superoxide disproportionation has been recently shown by $^{18}O_2/^{16}O_2$ isotopic experiments.[31]

Only a few studies reported the effect of lithium ion concentration on LiO_2 solubility in O_2 reduction in aprotic solvents[23] and the formation of Li_2O_2 deposit on the electrode by Raman spectroscopy.[27] The present study shows the effect of increasing the Li^+ ion concentration in DMSO containing $TBAPF_6$ and LiTFSI electrolytes on the stability of soluble superoxide, the deposition of insoluble Li_2O_2, the formation of singlet oxygen and the degradation of the solvent to Li_2CO_3 and CO_2 evolution upon oxidation. Furthermore, the selective deactivation of singlet oxygen by sodium azide shows complete charge recovery in a deep discharge-charge cycle of a Li–O_2 battery cathode.

Results and Discussion

It is well accepted the existence of two ORR mechanisms in lithium containing DMSO electrolytes, namely a solution phase and a surface pathway with a branching at the superoxide intermediate as shown in Scheme I.[22,23,35,36] However, there is recent evidence that most of the reaction goes through the DISP mechanism.[37]

In the present study the transition from $\left[TBA^+O_2^-\right]_{DMSO}$ to $[Li^+O_2^-]_{DMSO}$ has been studied by increasing the fraction ($0 \leq y \leq 1$) of lithium ions in electrolytes containing $yLiPF_6 + (1\text{-}y)\ TBAPF_6$ by several techniques: CV, RRDE, EQCM, DEMS and detection of singlet oxygen by DMA endo-peroxide fluorescence quenching.

The one-electron transfer to molecular oxygen yields soluble superoxide radical anion that forms an ion pair with TBA^+ or Li^+ respectively.

Dimethyl sulfoxide (DMSO) is a good electron donor (Gutnam DN 29.8)[38] and strongly coordinates Li^+[19] and thus stabilizes soluble $\left[Li^+O_2^-\right]_{DMSO}$ ion pairs, which can either disproportionate to yield Li_2O_2 and O_2, or undergo a further electron transfer via LiO_2*[32] to yield Li_2O_2, or diffuse away from the electrode surface into the liquid electrolyte. This branching point of the ORR mechanism has been studied with rotating ring disc electrode (RRDE), with an Au ring that collects a fraction of the superoxide generated at the disc surface.[21,22] In the absence of Li^+ or at very low concentration a quantitative collection of O_2^- at the Au ring electrode from the oxygen reduction at the disc electrode is observed, (i.e. $I_R = I_D N_0$) as depicted in Figure 1A for 1 mM $LiPF_6$. These results are in agreement with previous work.[20,23,39]

However, when the lithium ion concentration is above twice the O_2 solubility in DMSO and thus the superoxide concentration, i.e. ≥ 2 mM the EQCM shows mass increase in spite of a single peak in the cyclic voltammetry (see Figure SI. 2b). Figure 1B depicts RRDE curves for O_2 saturated in DMSO containing 100 mM $LiPF_6$ electrolyte. Only a small fraction of

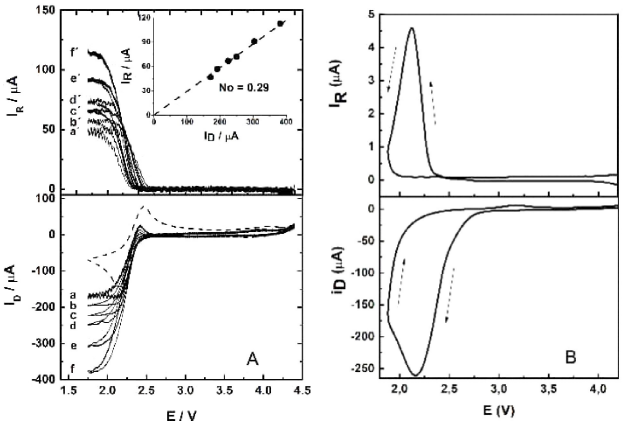

Figure 1. A. O_2 reduction polarization curve on an Au ($A_D = 0.2\ cm^2$) disk electrode in O_2 (1 atm) saturated 1 mM $LiPF_6$ in anhydrous DMSO at W = 0, 2, 3, 4, 5, 9, and 25 Hz and scan rate of 0.1 V.s (lower panel) and O_2^- oxidation Au ring currents at $E_R = 3$ V (upper panel). Inset shows collection efficiency. B. 100 mM $LiPF_6$ in anhydrous DMSO at W = 16 Hz and scan rate of 0.1 $V\,s^{-1}$ (lower panel) and RRDE Au ring ($N_0 = 0.29$, upper panel) superoxide oxidation current at $E_R = 3.0$ V.

soluble O_2^- formed by ORR is collected at the ring electrode, i.e 9% when the disk current reaches a peak below the convective-diffusion current. The same trend was observed in LiTFSI dissolved in $Pyr_{14}TFSI$ ionic liquid with a larger O_2 solubility, i.e. 13.6 mM. The peak is due to formation of an insoluble Li_2O_2 blocking film on the Au surface, i.e. supporting the surface mechanism.[21,40,41]

Superoxide is stable in the presence of large cations such as TBA^+, but in the presence of Li^+ ions disproportionation yields Li_2O_2 insoluble in DMSO and O_2.[26] The formation of a solid at the cathode surface has been studied gravimetrically at different lithium ion concentrations with the electrochemical quartz crystal microbalance (EQCM).[42] The cyclic voltammetry of the ORR on Au electrode in DMSO containing different concentrations of y $LiPF_6$ + (1-y) $TBAPF_6$ are shown in Figure SI1 for $0 \leq y \leq 100$ mM.

The cyclic voltammetry shows that in the absence of lithium ions (100 mM TBA) a reversible one-electron wave for the O_2/O_2^- couple is observed as reported elsewhere.[23,40] The simultaneous gravimetric EQCM shows a slight mass increase in the cathodic polarization which is recovered in the reverse scan, which can be ascribed to $[TBA^+O_2^-]_{DMSO}$ at the electrode surface (Figure S.I. 2).

At very low lithium ion concentration, below 2 mM Li^+ a single one-electron O_2 reduction peak to O_2^- and a superoxide oxidation peak is still observed in the back scan at 2.6 V (See Figure SI.2b). The solubility of O_2 in DMSO containing Li^+ is 2 mM[41] which determines the maximum concentration of superoxide at the cathode surface. Above 5 mM $LiPF_6$ the anodic peak due to superoxide re-oxidation disappears and a second anodic peak is apparent in the back scan above the O_2/Li_2O_2 redox potential, i.e. 2.96 V as can be seen in Figure 2 (see also Figure SI. 3 and 4).

The peak above 2.96 V corresponds to the oxidation of surface Li_2O_2 as has been demonstrated by DEMS[6] and Raman spectroscopy.[27] The simultaneous mass recorded by EQCM increases from the onset of the ORR and the mass uptake

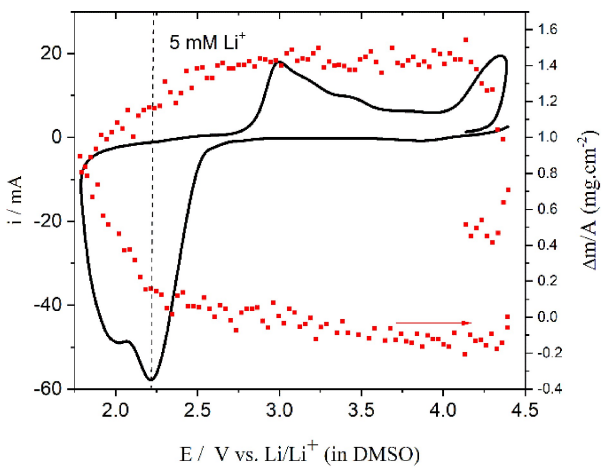

Figure 2. Cyclic voltammetry of O_2 (1 atm) reduction on Au (A = 0.20 cm^2) on a quartz crystal in: 5 mM $LiPF_6$ and 95 mM $TBAPF_6$ in DMSO, at 20 mV s^{-1} and simultaneous EQCM Δm/A.

becomes steeper after the second reduction peak due to the 2-electron transfer to form Li_2O_2 that is consistent with the decay of superoxide detected with the RRDE experiments. Also for Li^+ concentrations larger than 5 mM passivation of the Au surface with negligible current in the back scan is observed due to the formation of a thin non-conducting Li_2O_2 blocking film. These results are consistent with those reported by Sharon et. al.[17]

Therefore, above a critical Li^+ concentration, larger than twice the oxygen solubility, insoluble Li_2O_2 completely blocks the surface for the cathodic reduction of oxygen as reported before.[23,27] Yu and Ye[27] studied the same system with in situ Raman spectroscopy as a function of lithium ion concentration in 0.1 M $TBAClO_4$-DMSO at different electrode potential. The potential dependence of the Li_2O_2 signal at 788 cm^{-1} showed that even at 1 mM Li-ions a clear Raman evidence of peroxide deposit at the surface could be observed with an onset at the potential of the first cathodic peak of the ORR. This is consistent with the present gravimetric results depicted in Figure 2.

Increasing the lithium ion concentration above 5 mM, a second reduction peak at lower potential (2.0 V) is observed (SI Figure S3) associated to the two-electron formation of Li_2O_2 as previously reported by Johnson et. al. and Yu and Ye.[23,27] At 20 mM and above only one reduction peak is apparent (SI Figure S4) which shifts to more positive potentials increasing lithium ion concentration since the two-electron O_2 reduction requires two Li^+ ions for the formation of Li_2O_2[27] as shown by the RRDE lithium ion flux measurement.[43]

The transition of the reversible O_2/O_2^- to the O_2/Li_2O_2 system is reflected by the potential shift of the second peak to larger potential values between 5–100 mM Li^+.[23]

The low areal mass and full passivation are evidence of a thin film deposited on the electrode surface under cyclic voltammetry conditions. Based on the density value $\rho_{Li2O2} = 2.3\ g\,cm^{-3}$ and the gravimetric results the thickness of the Li_2O_2 blocking film results in the order of 5 nm as reported previously.[44]

Notice that the mass deposited on the surface does not decrease until above 4.3 V in spite of the decrease of the peroxide Raman signal at 788 cm^{-1} which totally decays at 3.6 V as shown by Yu and Ye.[27] Therefore, the surface solid mass observed by EQCM should consist mainly of spurious reaction products from solvent and electrolyte degradation and not Li_2O_2.

The other pathway in Scheme I leading to Li_2O_2 is the solution phase mechanism that is favoured at low current density. High donor number solvent and the presence of water traces favour the solution phase mechanism.[22,23,45]

Figure 3 illustrates the increase of the Li_2O_2 mass on the surface in a 10 μA constant current discharge as the Li^+ concentration in the electrolyte increases due to an enhancement of the superoxide disproportionation and consequently a decrease in the superoxide collected with the RRDE experiment (Figure 1).

The increase in Li_2O_2 mass during ORR and the decrease during the OER in current pulses at 1 and 10 mM $LiPF_6$/DMSO respectively under 5 μA cm^{-2} are depicted in Figure 4. At 1 mM and low current density (5 μA cm^{-2}) there is a time lag

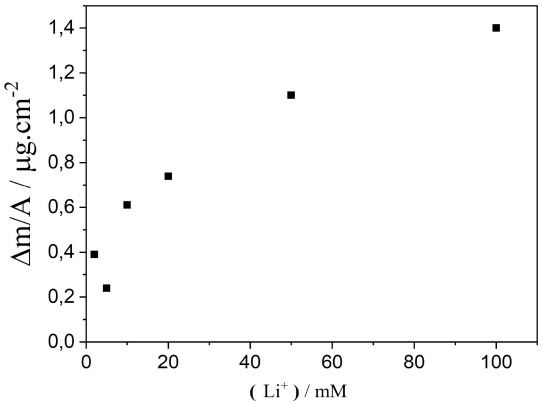

Figure 3. Maximum EQCM areal mass after a 10 μA pulse for the ORR on Au as a function of $LiPF_6$ concentration in DMSO.

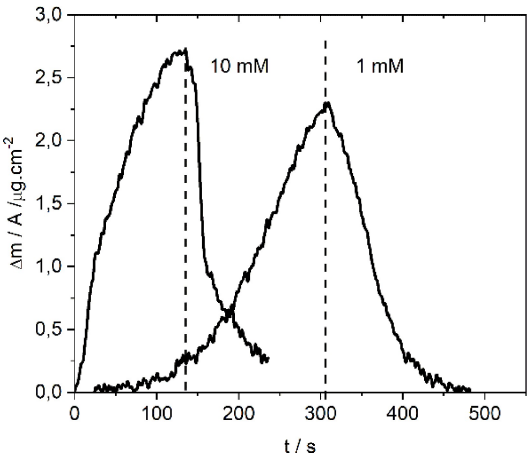

Figure 4. Time evolution of EQCM areal mass (Δm/A) during constant current of 5 μA cm^{-2} ORR and OER pulses respectively in 1 and 5 mM $LiPF_6$ in DMSO.

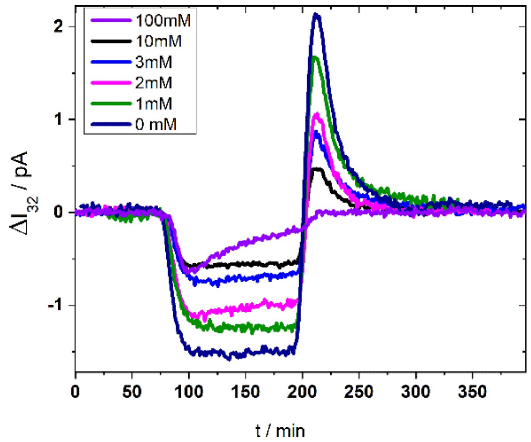

Figure 5. Simultaneous DEMS ionic current I_{32} for mass/charge = 32, during ORR and OER to a double chronoamperometry pulse for the O_2 electrode on Au sputtered PTFE (Teflon®) membrane of the DEMS cell in different lithium ion concentrations: x $LiPF_6$ + (1-x) $TBAPF_6$ in DMSO with $0 \le x \le 100$ mM at 1.9 V (ORR) and 3.1 V (OER).

characterized by soluble superoxide concentration build up in the solution adjacent to the oxygen cathode followed by a mass uptake due to deposition of insoluble Li_2O_2 resulting from O_2^- disproportionation. However, at higher lithium ion concentration, i.e. 10 mM a faster mass uptake is seen as has been shown previously at low and high current densities due to a contribution from solution phase mechanism.[42]

In the latter case higher superoxide concentration results in fast deposition of Li_2O_2 via disproportionation. The similar final mass at both concentrations is probably due to passivation of the surface by an insoluble and insulating layer of lithium peroxide that prevents further deposition.

While soluble superoxide was collected by the RRDE and lithium peroxide mass was measured by the EQCM, the depletion of oxygen during ORR and evolution upon oxidation was studied by differential electrochemical mass spectrometry (DEMS). Figure 5 shows simultaneous DEMS transients for O_2 (m/e = 32) during discharge and charge of the O_2 cathode at increasing Li^+ concentration.

In lithium free $TBAPF_6$/DMSO electrolyte a depletion of oxygen during ORR from the I_{32} ionic current is observed and a positive I_{32} ion current peak at 3.1 V due to the quantitative oxidation of surface superoxide which yields a collection efficiency for the DEMS cell of 0.3 (see SI Figure S10). Increasing the lithium concentration, less oxygen is depleted as detected by the constant I_{32} ionic current in the mass spectrometer, and at 100 mM $LiPF_6$ the I_{32} ionic current drops as the surface becomes blocked by solid products with negligible evolution of O_2 at 3.1 V consistent with cyclic voltammetry, EQCM and RRDE.

The oxidation of soluble superoxide on the Au/PTFE porous membrane surface at 3.1 V permeates oxygen into the vacuum mass spectrometer and results in an I_{32} peak that also decreases at increasing Li^+ concentration. Notice that no peak can be seen for 100 mM lithium ion concentration consistent with the EQCM and RRDE results.

Comparison of the electrochemical Faraday charge and DEMS mass (I_{32}) during superoxide oxidation was obtained from the mass spectrometry integrated charge using the calibration constant for the system (see S.I. Figure S10). Figure 6 shows the number of electrons involved per O_2 molecule during oxidation at different lithium ion concentration and 3.1 V and 3.7 V respectively.

These results show that below 5 mM the ORR proceeds mainly by the one-electron per O_2 molecule reaction as expected for the formation of superoxide ion, which is oxidized at 3.1 V. At higher lithium concentration two electrons per oxygen molecule are apparent since oxidation of lithium peroxide occurs at 3.7 V that is consistent with the lower yield of superoxide detected with the RRDE.

The increase in the EQCM mass due to Li_2O_2 deposition during ORR on Au in $LiPF_6$-Au at high lithium concentrations is consistent with less oxygen depletion shown by DEMS since peroxide on the surface blocks the ORR reaction. Yu and Ye have shown that in the oxidation back sweep of a cyclic voltammetry a decrease of the peroxide Raman signal at 788 cm^{-1} is observed from 2.0 V and total disappearance occurs at 3.6 V. In the present work. However, the EQCM mass

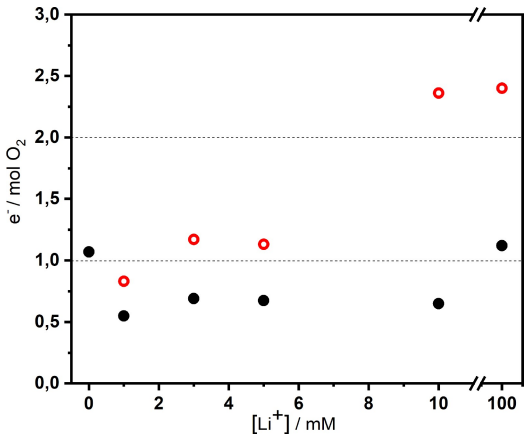

Figure 6. Number of electrons per O_2 molecule versus the $LiPF_6$ concentration in solution for oxidation at 3.10 (filled circles) and 3.70 V (open circles) respectively, obtained from DEMS experiments.

decreases just above these potentials for the different lithium concentrations and therefore we conclude that the surface deposit consists of by-products from spurious reactions in addition to Li_2O_2 formation.

Superoxide disproportionation requires high local concentration to reach a substantial rate and the presence of lithium ions enhances the O_2^- disproportionation.[26] It is also well accepted that disproportionation of alkaline superoxides yields singlet oxygen ($^1O_2$ or $^1\triangle_g$) as well as triplet oxygen ($^3O_2$ or $3\Sigma_g-$).[46] Singlet oxygen has been detected during discharge and charge of Li–O_2 battery cathodes. In a series of papers, the group of Freunberger has described the detection of singlet oxygen formed during cycling Li–O_2 and Na-O_2 battery cathodes using 9,10-dimethyl anthracene (DMA), which is stable in contact with superoxide and reacts rapidly and specifically with singlet oxygen to form an endo-peroxide (DMA-O_2). (See inset in Figure 7) The fluorescence emission of DMA at 430 nm decays upon reaction with singlet oxygen since the DMA-endoperoxide is non-fluorescent.[29,47]

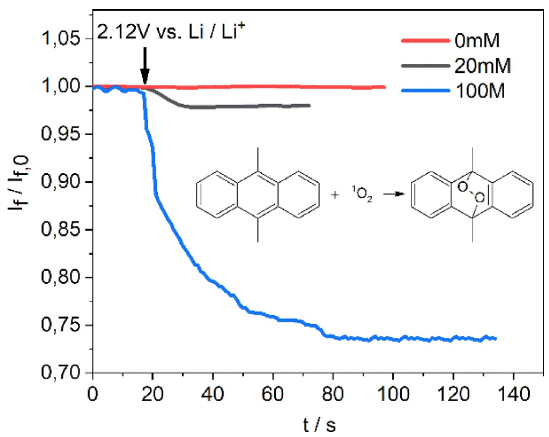

Figure 7. Fluorescence emission decay at 430 nm of 50 μM DMA during a chronoamperommetry of O_2 reduction at Au electrode at 2.12 V (vs. Li/Li^+) in O_2 saturated LiTFSI in DMSO electrolyte at different Li^+ concentrations: 0, 20 and 100 mM. Excitation wavelength 378 nm.

In the present study, DMA has been used as a specific detector of singlet oxygen formation by analyzing the fluorescence decay at 430 nm of 50 μM DMA during an O_2 reduction on Au chronoamperommetry at 2.12 V (vs. Li/Li^+) in oxygen saturated LiTFSI/DMSO electrolyte at different Li^+ concentrations: 0, 20 and 100 mM with excitation wavelength 378 nm (see Figure 7).

In the absence of O_2 in the electrolyte there was no change in the fluorescence emission of DMA when the Au electrode was polarized in the ORR potential region in Li containing electrolyte. When the electrolyte was saturated with O_2 in absence of lithium ions the fluorescence emission remained unchanged. However, when the O_2 saturated electrolyte contained increasing Li^+ ion concentrations there was a decrease in the fluorescence emission during the ORR chronopotentiometry at 2.12 V. The decrease in DMA fluorescence was larger the larger the Li^+ concentration as shown in Figure 7 following the trend in superoxide disproportionation and the peroxide mass increase.

Notice that in the experiments reported here the electrolyte was unstirred to enhance the sensitivity by keeping a relatively high local superoxide concentration on the Au electrode surface, and therefore to increase the $^1O_2$ formation via lithium superoxide disproportionation.[30]

Therefore, the superoxide disproportionation in the solution adjacent to the Au cathode yields $^1O_2$ which selectively forms DMA endo-peroxide and contributes to the observed fluorescence quenching as shown in Scheme 1.

Alternatively, we may consider disproportionation of adsorbed LiO_2* (Reaction 2)

$$[LiO_2^*]_{surf} + [LiO_2^*]_{surf} \rightarrow Li_2O_2 \downarrow + x^1O_2 + (1-x)^3O_2 \quad (2)$$

A theoretical calculation of the pathways to triplet or singlet oxygen during the dissociation of alkali superoxides has been published recently for the oxidation of Li_2O_2.[48] The disproportionation of superoxide involves a dimer transition state.[31,49]

The lifetime of $^1O_2$ in DMSO is 5.5 μs,[50] therefore DMA fluorescence quenching arises from the solution adjacent to the Au cathode since the extremely reactive oxygen excited species would react with DMSO in spurious reactions for the Li–O_2 cathode.

The effect of lithium ion on the spurious reactions during the ORR has been studied by DEMS ΔI_{44} signals simultaneously to the O_2 reduction on a porous Au/Teflon membrane. The

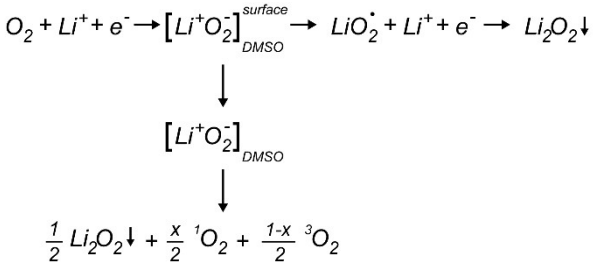

Scheme 1. ORR Scheme at Au electrode in Li^+-DMSO electrolyte.

oxidation of superoxide at 3.1 V and other surface ORR products at 3.7 V respectively can be seen in Figure 8.

In the absence of Li^+ in the electrolyte, no evidence of CO_2 evolution can be observed. However, for as low as 5 mM lithium ion concentration there is a clear evolution of CO_2 at 3.7 V, lower than the onset potential for the electrochemical oxidation of DMSO.[16,51] Since the only source of carbon is the electrolyte, CO_2 should result from the product of spurious decomposition reactions involving ORR reactive products in the presence of lithium ions, i.e. singlet oxygen from disproportionation of superoxide.

At 3.1 V only the release of oxygen is observed with no evolution of CO_2, but at 3.7 V CO_2 evolution occurs. Probably lithium carbonate detected by XPS on this surface and removed above 3.7 V[51] releases CO_2.

We conclude that only in the presence of lithium in the electrolyte CO_2 is released from the decomposition of surface lithium carbonate formed by reaction of singlet oxygen with the solvent.

We have recently shown that singlet oxygen formed by disproportionation of lithium superoxide in Li–O_2 battery cathodes with LiTFSI-DMSO electrolyte can be efficiently quenched by azide ions,[30] which is a selective physical quencher of $^1O_2$. Preliminary results of constant current charge–discharge of a full Li–O_2 battery with and without sodium azide added in the electrolyte are shown in Figure 9.

A current density of 0.1 mA cm^{-2} was applied to the battery with charging cut off potential of 4.3 V below the solvent decomposition potential[16] and discharge cut off potential of 2.0 V to a complete discharge of the battery.

Unlike in limited depth of discharge,[52] in full discharge-charge curves in DMSO electrolyte the electrical charge during discharge is never recovered in successive charge cycles due to spurious reactions and formation of decomposition surface products.[53]

The Li–O_2 battery with LiTFSI/DMSO but no azide added to the electrolyte showed the same discharge voltage plateau as the battery with azide additive in the electrolyte but a smaller capacity as depicted in Figure 9. Furthermore, upon charging at the cut off potential of 4.3 V only a fraction of the charge delivered in the discharge half cycle could be recovered in the first charging cycle and upon repetitive cycles capacity fading was observed as reported before.[54]

The reversibility of the Li–O_2 battery has never reached more than 80% due to parasitic reactions as shown by the ratio of evolved to consumed O_2 in a round discharge-charge cycle[6] and highly reactive singlet oxygen ($^1O_2$) is now recognized as the major driver of parasitic chemistry. Azide ion efficiently suppresses singlet oxygen by physical quenching, therefore it is expected that addition of azide to the electrolyte would result in the absence of surface by-products from electrolyte and solvent degradation with more reversible chemistry of the Li–O_2 battery.

The mechanism for singlet oxygen production still has critical open questions that can be answered by combination of different experimental techniques.

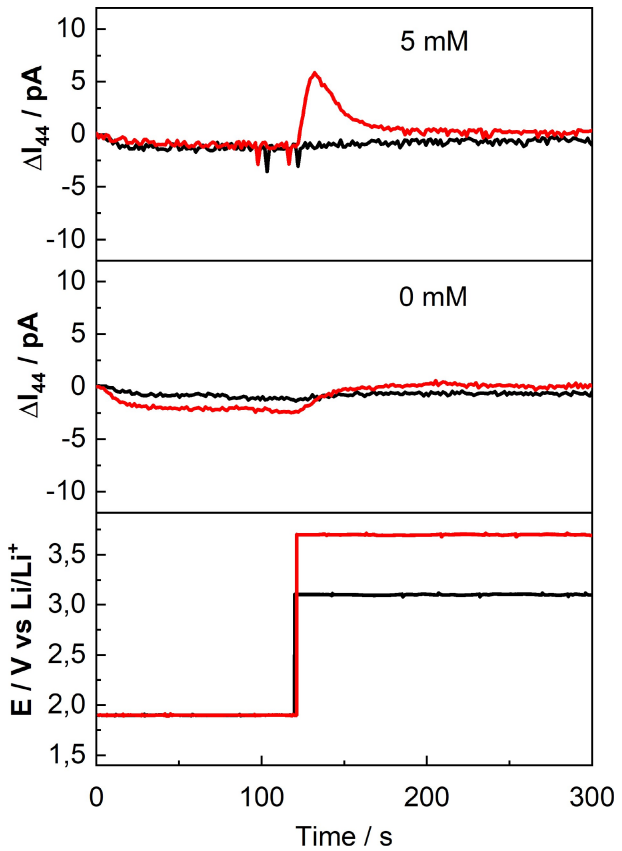

Figure 8. Simultaneous DEMS ionic current difference ΔI_{44} transients during ORR and OER to a double chronoamperometry pulse for the O_2 electrode on Au sputtered PTFE (Teflon®) membrane at 1.9 V (ORR), 3.1 V (black) and 3.7 V (red) OER and $LiPF_6$ concentrations 0 and 5 mM respectively.

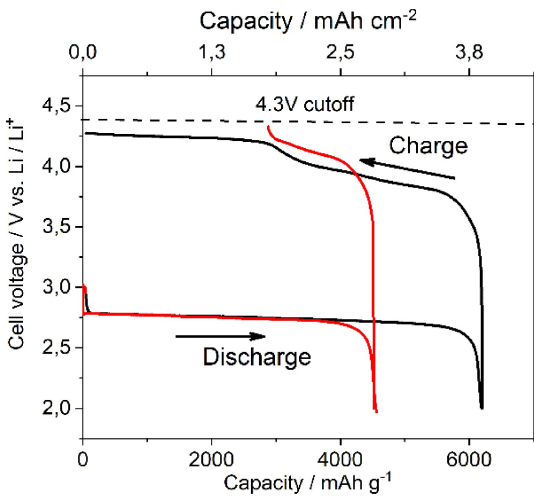

Figure 9. Full discharge-charge cycle of a Li–O_2 battery with a lithium foil anode and 0.5 mg Vulcan XC-72 (Cabot®) on carbon paper cathode with a Whatman separator in O^2 saturated 1 M LiTFSI/DMSO electrolyte (red curve) and with the addition of 30 mM NaN_3 (black curve). Cut-off potential: 4.3 V vs. Li/Li^+ (DMSO). Current density: 0.1 mA/cm^2.

Conclusion

The role of superoxide disproportionation on the formation of the reactive singlet oxygen species upon increasing the lithium ion concentration in DMSO electrolyte has been shown by combination of various in-situ techniques. Further participation of the reactive singlet oxygen in spurious solvent degradation reactions and deactivation by sodium azide has enabled Li–O_2 cathodes with full charge recovery in deep charge-discharge cycles.

Experimental Section

CHEMICALS. Anhydrous dimethyl sulfoxide (DMSO), $\geq$99.9%, $LiPF_6$ battery grade, $\geq$99.99% were obtained from SIGMA-ALDRICH and stored in the argon-filled MBRAUN glove box with the oxygen content $\leq$0.1 ppm and water content below 2 ppm. DMSO was dried for several days over molecular sieves, 3 Å (Sigma-Aldrich). All solutions were prepared inside the glove box and the water content was measured using the Karl Fisher 831 KF Coulometer (Metrohm) with typically 50 ppm of water.

RRDE: A rotating ring disk electrode (RRDE) with Au disk and Au ring electrodes embedded in an Araldite epoxy resin cylindrical body (Ciba-Geigy) was employed as described elsewhere.[22] The geometry parameters of the system were $r_1 = 0{,}25$ cm, $r_2 = 0.26$ cm and $r_3 = 0.30$ cm with a disk area $A = 0.2\ cm^2$ and a geometric collection efficiency $N_0 = 0.29$ was calculated using the Albery-Hitchman theory[55] and experimentally verified with the redox couple $K_3Fe(CN)_6$/ $K_4Fe(CN)_6$, $N_0 = 0.28$. For the detection of superoxide at the Au ring electrode at ring potential $E_R = 3.0$ V (vs Li/Li^+ in DMSO) was applied as reported elsewhere.[22]

Differential electrochemical mass spectrometry (DEMS) was accomplished using a Pfeiffer vacuum Omnistar GSD 320 gas analysis system with a base pressure of 10^{-8} mbar with a quadrupole mass spectrometer (mass range 1–200 amu) with ion gas tight ion source, yttriated iridium-filament with secondary electron multiplier C-SEM and Faraday detectors. The DEMS cell setup was a modification of the design pioneered by Baltruschat et al.[56,57] and consisted of a stainless steel base with a PTFE body. A gold sputtered PTFE membrane gas diffusion electrode (200 μm thick and 0.1 μm pore diameter T01047WPH Microclar Teflon) with 0.50 cm^2 geometric electroactive area located at the bottom of the cell. The Au sputtered membrane was mechanically supported on a porous stainless steel frit. Surface tension of the solvent DMSO (43.5 $mN\,m^{-1}$) prevents penetration in the capillary porous structure of the PTFE membrane.[58] The electrolyte-vacuum interface was connected to the gas analyzer by 1/8″ stainless steel tubing through an on/off valve, which was opened when the pressure dropped below 10 mbar. Details of calibrations can be found in the Supplementary Information.

Electrochemical Quartz Crystal Microbalance (EQCM): Crystal admittance spectra in the vicinity of the fundamental resonant frequency, f_o were acquired using a Hewlett Packard HP E5100A network analyser connected to the quartz crystal in the electrochemical cell through 50 Ω coaxial matched cables via a HP 41900A. EQCM data acquisition and data analysis has been described elsewhere.[42] The electrochemical cell is described in the Supplementary Information.

Singlet oxygen detection: In-operando detection of $^1O_2$ during oxygen reduction in DMSO-LiTFSI electrolyte was detected by DMA fluorescence quenching in unstirred electrolyte as described elsewhere[30] (see Figure SI 11 details therein).

Li–O_2 battery: A home-made cell similar to Electrocell was used (see Figure SI. 12) which consisted of a 10 mm diameter Li foil disc in contact with a 250 μm Whatman glass fibre separator embedded in 150 μL of 1 M LiTFSI electrolyte in DMSO. A 10 mm diameter gas diffusion layer (GDL) carbon paper (Freudenberg H23C4, 0.7 m^2/g) with 0.5 mg of Vulcan XC-72 (Cabot®) and poly(vinylidene) fluoride (PVDF) binder (90:10) in N-Methyl-2-pyrrolidone was employed as the working cathode.

Acknowledgements

Funding from CONICET and ANPCyT PICT 2014 No. 3654 and PIDDEF-36/16 and research doctoral fellowships from CONICET by DC and FD are gratefully

Conflict of Interest

The authors declare no conflict of interest.

Data Availability Statement

The data that support the findings of this study are available from the corresponding author upon reasonable request.

Keywords: Battery · Lithium · Oxygen · Singlet oxygen · Superoxide

[1] K. M. Abraham, Z. Jiang, *J. Electrochem. Soc.* **1996**, *143*, 1–5.
[2] K. M. Abraham, *ECS Trans.* **2008**, *3*, 67–71.
[3] J. Christensen, P. Albertus, R. S. Sanchez-Carrera, T. Lohmann, B. Kozinsky, R. Liedtke, J. Ahmed, A. Kojic, *J. Electrochem. Soc.* **2012**, *159*, R1-R30.
[4] D. Aurbach, B. D. McCloskey, L. F. Nazar, P. G. Bruce, *Nat. Energy.* **2016**, *1*, 16128.
[5] K. Amine, R. Kanno, Y. Tzeng, *MRS Bull.* **2014**, *39*, 395–401.
[6] A. C. Luntz, B. D. McCloskey, *Nat. Energy.* **2017**, *2*, 17056.
[7] W.-J. Kwak, Rosy, D. Sharon, C. Xia, H. Kim, L. R. Johnson, P. G. Bruce, L. F. Nazar, Y.-K. Sun, A. A. Frimer, M. Noked, S. A. Freunberger, D. Aurbach, *Chem. Rev.* **2020**, *120*, 6626–6683.
[8] Y. Zhang, X. Zhang, J. Wang, W. C. McKee, Y. Xu, Z. Peng, *J. Phys. Chem. C.* **2016**, *120*, 3698.
[9] W.-J. Kwak, J.-B. Park, H.-G. Jung, Y.-K. Sun, *ACS Energy Lett.* **2017**, *2*, 2756–2760.
[10] A. Halder, H.-H. Wang, K. C. Lau, R. S. Assary, J. Lu, S. Vajda, K. Amine, L. A. Curtiss, *ACS Energy Lett.* **2018**, *3*, 1105–1109.
[11] A. C. Luntz, B. D. McCloskey, *Chem. Rev.* **2014**, *114*, 11721–11750.
[12] N. B. Aetukuri, B. D. McCloskey, J. M. Garciá, L. E. Krupp, V. Viswanathan, A. C. Luntz, *Nat. Chem.* **2015**, *7*, 50–56.
[13] F. Marchini, S. Herrera, W. Torres, A. Y. Tesio, F. J. Williams, E. J. Calvo, *Langmuir* **2015**, *31*, 9236–9245.
[14] M. A. Schroeder, N. Kumar, A. Pearse, C. Liu, S. B. Lee, G. W. Rubloff, K. Leung, M. Noked, *ACS Appl. Mater. Interfaces* **2015**, *7 21*, 11402–11411.
[15] D. G. Kwabi, T. P. Batcho, C. V. Amanchukwu, N. Ortiz-Vitoriano, P. T. Hammond, C. V. Thompson, Y. Shao-horn, *J. Phys. Chem. Lett.* **2014**, *5(16)*, 2850–2856.
[16] N. Mozhzhukhina, L. P. MÃ©ndez De Leo, E. J. Calvo, *J. Phys. Chem. C* **2013**, *117*, 18375–18380.

[17] D. Sharon, M. Afri, M. Noked, A. Garsuch, A. A. Frimer, D. Aurbach, *J. Phys. Chem. Lett.* **2013**, *4*, 3115–3119.
[18] D. T. Sawyer, J. L. Roberts, *J. Electroanal. Chem.* **1966**, *12*, 90–101.
[19] R. Semino, G. Zaldívar, E. J. Calvo, D. Laria, *J. Chem. Phys.* **2014**, *141*, 214509.
[20] M. Trahan, S. Mukerjee, E. J. Plichta, M. A. Hendrickson, K. M. Abraham, *J. Electrochem. Soc.* **2013**, *160*, A259.
[21] E. J. Calvo, N. Mozhzhukhina, *Electrochem. Commun.* **2013**, *31*, 56–58.
[22] W. Torres, N. Mozhzhukhina, A. Y. Tesio, E. J. Calvo, *J. Electrochem. Soc.* **2014**, *161*, A2204-A2209.
[23] L. Johnson, C. Li, Z. Liu, Y. Chen, S. A. Freunberger, P. C. Ashok, B. B. Praveen, K. Dholakia, J.-M. Tarascon, P. G. Bruce, *Nat. Chem.* **2014**, *6*, 1091–1099.
[24] J. Herranz, A. Garsuch, H. A. Gasteiger, *J. Phys. Chem. C* **2012**, *116*, 19084–19094.
[25] J. T. Frith, A. E. Russell, N. Garcia-Araez, J. R. Owen, *Electrochem. Commun.* **2014**, *46*, 33–35.
[26] M. Del Pozo, W. R. Torres, S. E. Herrera, E. J. Calvo, *ChemElectroChem* **2016**, *3*, 1537–1540.
[27] Q. Yu, S. Ye, *J. Phys. Chem. C* **2015**, *119*, 12236–12250.
[28] J. Wandt, P. Jakes, J. Granwehr, H. A. Gasteiger, R.-A. Eichel, *Angew. Chem. Int. Ed.* **2016**, *55*, 6892–6895; *Angew. Chem.* **2016**, *128*, 7006–7009.
[29] N. Mahne, B. Schafzahl, C. Leypold, M. Leypold, S. Grumm, A. Leitgeb, Gernot A. Strohmeier, M. Wilkening, O. Fontaine, D. Kramer, C. Slugovc, Sergey M. Borisov, Stefan A. Freunberger, *Nat. Energy.* **2017**, *2*, 17036.
[30] D. Córdoba, H. B. Rodríguez, E. J. Calvo, *ChemistrySelect* **2019**, *4*, 12304–12307.
[31] S. Dong, S. Yang, Y. Chen, C. Kuss, G. Cui, L. R. Johnson, X. Gao, P. G. Bruce, *Joule.* **2022**, *6*, 185–192.
[32] X. Zhang, L. Guo, L. Gan, Y. Zhang, J. Wang, L. R. Johnson, P. G. Bruce, Z. Peng, *J. Phys. Chem. Lett.* **2017**, *8*, 2334–2338.
[33] A. T. S. Freiberg, M. K. Roos, J. Wandt, R. de Vivie-Riedle, H. A. Gasteiger, *J. Phys. Chem. A.* **2018**, *122*, 8828–8839.
[34] W.-J. Kwak, H. Kim, Y. K. Petit, C. Leypold, T. T. Nguyen, N. Mahne, P. Redfern, L. A. Curtiss, H.-G. Jung, S. M. Borisov, S. A. Freunberger, Y.-K. Sun, *Nat. Commun.* **2019**, *10*, 1380.
[35] Y. Wang, Y.-C. Lu, *Energy Storage Mater.* **2020**, *28*, 235–246.
[36] G. Houchins, V. Pande, V. Viswanathan, *ACS Energy Lett.* **2020**, *5*, 1893–1899.
[37] C. Prehal, S. Mondal, L. Lovicar, S. A. Freunberger, *ACS Energy Lett.* **2022**, *7*, 3112–3119.
[38] V. Gutmann, *Coord. Chem. Rev.* **1976**, *18*, 225–255.
[39] W. R. Torres, A. Y. Tesio, E. J. Calvo, *Electrochem. Commun.* **2014**, *49*, 38–41.
[40] C. O. Laoire, S. Mukerjee, K. M. Abraham, E. J. Plichta, M. A. Hendrickson, *J. Phys. Chem. C* **2009**, *113*, 20127–20134.
[41] C. O. Laoire, S. Mukerjee, K. M. Abraham, E. J. Plichta, M. A. Hendrickson, *J. Phys. Chem. C* **2010**, *114*, 9178–9186.
[42] W. R. Torres, L. Cantoni, A. Y. Tesio, M. del Pozo, E. J. Calvo, *J. Electroanal. Chem.* **2016**, *765*, 45–51.
[43] M. D. del Pozo, F. Marchini, L. Cantoni, E. J. Calvo, *Electrochim. Acta* **2019**, *296*, 901–906.
[44] V. Viswanathan, K. S. Thygesen, J. S. Hummelshøj, J. K. Nørskov, G. Girishkumar, B. D. McCloskey, A. C. Luntz, *J. Chem. Phys.* **2011**, *135*, 214704.
[45] B. D. Adams, C. Radtke, R. Black, M. L. Trudeau, K. Zaghib, L. F. Nazar, *Energy Environ. Sci.* **2013**, *6*, 1772–1778.
[46] C. P. Andrieux, P. Hapiot, J.-M. Savéant, *J. Am. Chem. Soc.* **1987**, *109*, 3768–3775.
[47] N. Mahne, O. Fontaine, M. O. Thotiyl, M. Wilkening, S. A. Freunberger, *Chem. Sci.* **2017**, *8*, 6716–6729.
[48] A. Zaichenko, D. Schröder, J. Janek, D. Mollenhauer, *Chemistry* **2020**, *26*, 2395–2404.
[49] A. Pierini, S. Brutti, E. Bodo, *Comp. Mat.* **2021**, *7*, 126, DOI. https://doi.org/10.1038/s41524-021-00597-3.
[50] J. Varchola, K. Želonková, D. Chorvat, D. Jancura, P. Miškovský, G. Bánó, *J. Lumin.* **2016**, *177*, 17–21.
[51] N. Mozhzhukhina, F. Marchini, W. R. Torres, A. Y. Tesio, L. P. Mendez De Leo, F. J. Williams, E. J. Calvo, *Electrochem. Commun.* **2017**, *80*, 16–19.
[52] B. Sun, X. Huang, S. Chen, J. Zhang, G. Wang, *RSC Adv.* **2014**, *4*, 11115–11120.
[53] H. Wang, K. Xie, *Electrochim. Acta.* **2012**, *64*, 29–34.
[54] B. D. McCloskey, A. Valery, A. C. Luntz, S. R. Gowda, G. M. Wallraff, J. M. Garcia, T. Mori, L. E. Krupp, *J. Phys. Chem. Lett.* **2013**, *4*, 2989–2993.
[55] W. J. Albery, M. L. Hitchman, *Trans. Faraday Soc.* **1971**, *67*, 2408–2413, DOI. https://doi.org/10.1039/TF9686402831.
[56] A. A. Abd-El-Latif, C. J. Bondue, S. Ernst, M. Hegemann, J. K. Kaul, M. Khodayari, E. Mostafa, A. Stefanova, H. Baltruschat, *TrAC Trends Anal. Chem.* **2015**, *70*, 4–13.
[57] A. E. A. A. A. Abd-El-Latif, J. Xu, N. Bogolowski, P. Königshoven, H. Baltruschat, *Electrocatalysis* **2011**, *3*, 39–47.
[58] S. J. Ashton, *Design, Construction and Research Application of a Differential Electrochemical Mass Spectrometer (DEMS)*, Springer, Berlin, New York Technical University of Munich, **2012**.

Manuscript received: October 13, 2022
Revised manuscript received: October 18, 2022